NANO LETTERS

Letter

pubs.acs.org/NanoLett

High-Yield Production of MoS_2 and WS_2 Quantum Sheets from Their Bulk Materials

Chunchun Han,[†] Yong Zhang,*[,†,‡] Peng Gao,[∥] Shulin Chen,[∥,§] Xinfeng Liu,[#] Yang Mi,[#] Jianqi Zhang,[†] Yanhong Ma,[†] Wenyu Jiang,[†] and Jinquan Chang[†]

[†]CAS Key Laboratory of Nanosystem and Hierarchical Fabrication, CAS Center for Excellence in Nanoscience, National Center for Nanoscience and Technology, Beijing 100190, P. R. China

[‡]University of Chinese Academy of Sciences, Beijing 100049, P. R. China

[∥]Electron Microscopy Laboratory and International Center for Quantum Materials, School of Physics, Peking University, Beijing 100871, P. R. China

[§]State Key Laboratory of Advanced Welding and Joining, Harbin Institute of Technology, Harbin 150001, P. R. China

[#]CAS Key Laboratory of Standardization and Measurement for Nanotechnology, CAS Center for Excellence in Nanoscience, National Center for Nanoscience and Technology, Beijing 100190, P. R. China

S *Supporting Information*

ABSTRACT: Mass production of two-dimensional quantum sheets (2D QSs) is highly desired to fully exploit their properties. Herein, we present a general strategy for the high-yield production of molybdenum disulfide (MoS_2) and tungsten disulfide (WS_2) QSs by a sequential combination of salt-assisted ball-milling and sonication-assisted solvent exfoliation of their bulk materials. Such a strategy enables reproducible production of intrinsic and defect-free MoS_2 and WS_2 QSs with exceedingly high yields of 25.5 and 20.1 wt %, respectively. By precipitation-redispersion treatment, the QSs can be redispersed in a wide range of solvents with redispersion concentration up to 20 mg/mL or even higher. Remarkable nonlinear absorption saturation is demonstrated in the QSs-poly(methyl methacrylate) (PMMA) hybrid thin film with loading content of merely 0.1 wt %. Our method provides an avenue toward mass production and full exploration of 2D QSs.

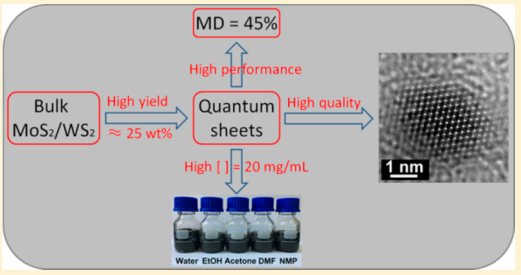

KEYWORDS: *Quantum sheets, TMDs, intrinsic, hybrid thin films, absorption saturation*

Two-dimensional (2D) materials have attracted much attention over the past ten years.[1−4] However, most of the research has focused on their micro/nanosheets (NSs).[2,3] Recently, 2D materials with further reduced dimensions, e.g., nanoribbons, quantum dots, and quantum sheets (QSs), have emerged.[5−7] With lateral sizes of approximately <20 nm,[6] QSs could be imparted with not only the intrinsic characteristic of 2D materials but also quantum confinement and prominent edge effects. It is therefore significant and imperative to produce and explore such emerging amazing 2D materials.[8−10] Meanwhile, transition metal dichalcogenides (TMDs) have shown extraordinary properties and potential applications.[11−14] As the most representative TMDs, molybdenum disulfide (MoS_2) and tungsten disulfide (WS_2) are intensively studied. Both bottom-up and top-down methods have been employed for the production of MoS_2 and WS_2 QSs. The former often suffers from rigorous conditions and tedious post-treatment,[15] whereas the latter usually produces QSs with extremely low yield.[16] Besides these drawbacks, another challenge toward the current fabrication methods is to obtain intrinsic QSs with negligible defects, which is a prerequisite to their full exploration.

Thanks to the abundance of bulk materials of TMDs, it would be very promising to produce MoS_2 and WS_2 QSs directly from their bulk materials. MoS_2 and WS_2 bulk materials have been revealed as layered structures in which a single layer consists of S−Mo−S and S−W−S chemically bonded atomic triplanes and adjacent layers stack through weak van der Waals interactions.[17] Evidently, the in-plane chemical bonds and interlayer van der Waals interactions have to be broken to transform the bulk materials into QSs. It has been reported that sonication and ball-milling, as well as grinding, can be used to exfoliate and pulverize the bulk 2D materials through breaking the van der Waals interactions and the chemical bonds, respectively.[18] However, the transformation of bulk materials into QSs is far from satisfactory by direct employment of the above methods. Inorganic materials have been introduced into the ball-milling/grinding process, which resulted in further exfoliated and pulverized 2D materials.[19−22] However, the resulting 2D materials are essentially nanosheets with polydispersed sizes and functionalized edges.

Received: September 15, 2017
Revised: November 7, 2017
Published: November 17, 2017

DOI: 10.1021/acs.nanolett.7b03968
Nano Lett. 2017, 17, 7767−7772

To date, there is still lacking a method for the mass production of intrinsic QSs of TMDs. Herein, we report a general strategy for the high-yield production of MoS_2 and WS_2 QSs with intrinsic and defect-free characteristics, which was achieved by sequential combination of salt-assisted ball-milling and sonication-assisted solvent exfoliation of the bulk materials. With such a strategy, intrinsic and defect-free MoS_2 and WS_2 QSs were produced with extremely high yields of 25.5 and 20.1 wt %, respectively. The QSs could be redispersed in a wide range of solvents with a redispersion concentration up to 20 mg/mL or even higher. The QSs-poly(methyl methacrylate) (PMMA) hybrid thin film with loading content of merely 0.1 wt % showed extraordinary nonlinear absorption saturation with modulation depth of approximately 45%, nearly an order of magnitude enhancement to that of NSs-PMMA.

The fabrication process of the MoS_2 and WS_2 QSs was illustrated in Figure 1a. It should be stated that dry milling rather than wet milling was employed to maximize the pulverization of the bulk materials. The introduction of inorganic salts such as sodium chloride (NaCl) and many others (see Table S2) into the ball-milling process played a key role as well. Such salt-assisted ball-milling pushed the pulverization to an unprecedented level (see Figures S3−S5). The following sonication-assisted solvent exfoliation transformed the pulverized materials into MoS_2 and WS_2 QSs. After filtration and centrifugation, highly stable dispersions of the QSs in *N*-methyl-2-pyrrolidone (NMP) were obtained.

A single cycle of the above fabrication process enabled production of MoS_2 and WS_2 QSs from their bulk materials with high yields of 25.5 and 20.1 wt %, respectively, which was 1−2 orders of magnitude higher than that reported previously.[16] Repeating the fabrication process could further improve the production yield. The MoS_2 and WS_2 QSs were characterized by transmission electron microscopy (TEM). As shown in Figure 1b and f, both QSs were well-dispersed without aggregation and were uniform in shape and size. The corresponding dispersions of the QSs in NMP appeared as dark green and dark red, respectively (insets of Figure 1b and f). Such appearance of the dispersions could imply the successful reduction of the lateral sizes and exfoliation of the bulk materials into QSs. Panels c and g in Figure 1 presented the size distributions of the QSs from which 4.9 ± 0.9 and 4.2 ± 1.0 nm were derived for MoS_2 and WS_2 QSs, respectively. The atomic force microscopy (AFM) characterization, as shown in Figure 1d and h, confirmed that the height of the MoS_2 QSs was 1.0 ± 0.5 nm, which indicated that the number of layers of MoS_2 QSs was 2 ± 1 layers because the thickness of single-layer MoS_2 was approximately 0.65 nm. Energy-dispersive X-ray (EDX) spectra, as in Figure 1e and i, showed the characteristic peaks of Mo and S for MoS_2 QSs and W and S for WS_2 QSs, respectively. No peaks for O were observed, indicating the nondestructive state of both QSs. The absence of the peaks for Na and Cl confirmed that the introduced salts were completely removed after thorough and repeated washing. It should be stated that the peaks of C and Cu originated from the supporting carbon film and copper grids.

State-of-the-art characterization tools were applied for the structural elucidation of the MoS_2 QSs. Figure 2a presents the high-resolution TEM (HRTEM) image of a single MoS_2 QS, which clearly reveals its hexagonal lattice structure.[14] The corresponding fast Fourier transform (FFT) pattern, as in Figure 2b, confirmed its single-crystalline characteristic. Figure 2c showed the UV−vis spectra of the MoS_2 QSs and NSs,

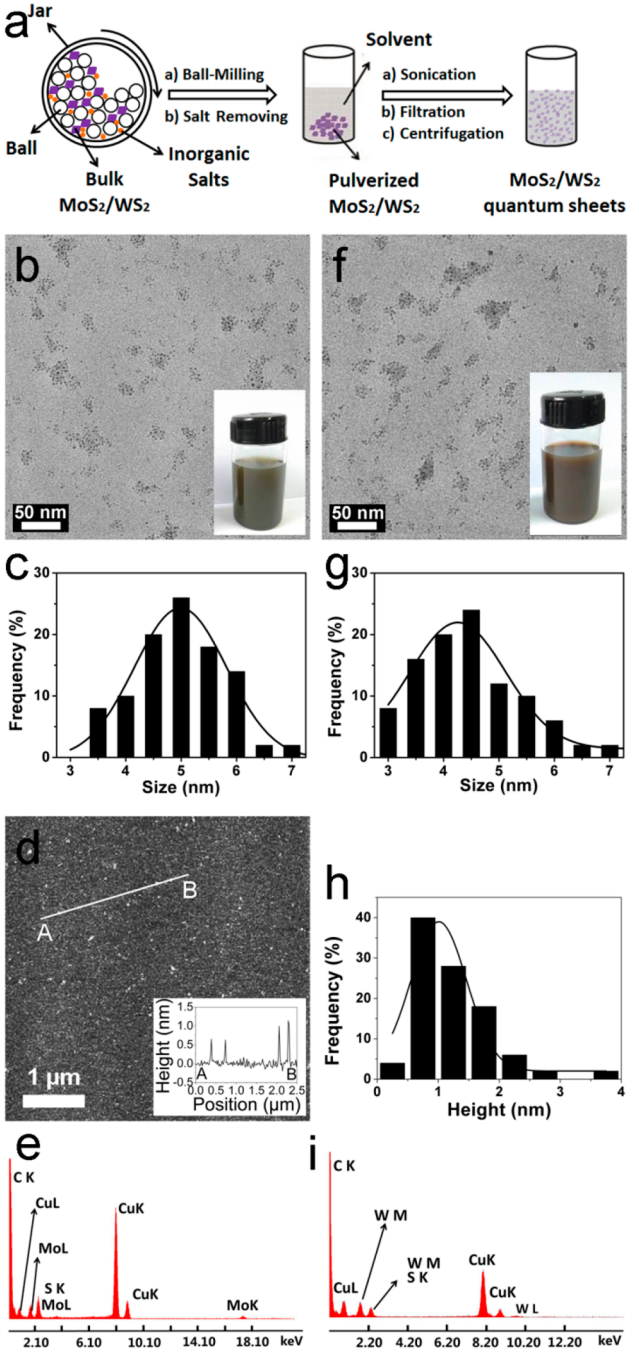

Figure 1. Fabrication and characterization of MoS_2 and WS_2 QSs. (a) Schematic illustration of the fabrication process. (b,f) TEM images, (c,g) size distributions, (d,h) AFM image and height distribution of MoS_2 QSs, and (e,i) EDX spectra for the MoS_2 and WS_2 QSs, respectively. Insets in (b) and (f) are photographs of the corresponding QS dispersions. Inset in (d) is the height profiles along the white line.

respectively. For the MoS_2 NSs, the peaks at 669 and 608 nm were attributed to the K point of the Brillouin zone, and the peaks at 396 and 457 nm were assigned to direct transition from the deep valence band to the conduction band. Conversely, for the MoS_2 QSs, the above characteristic peaks became implicit, and a blue-shifted peak at 330 nm was observed. Such phenomena demonstrated the prominent quantum confinement effect of the MoS_2 QSs.[23] Similar trends were found in the case of WS_2 (Figure S1). In the Raman

DOI: 10.1021/acs.nanolett.7b03968
Nano Lett. 2017, 17, 7767−7772

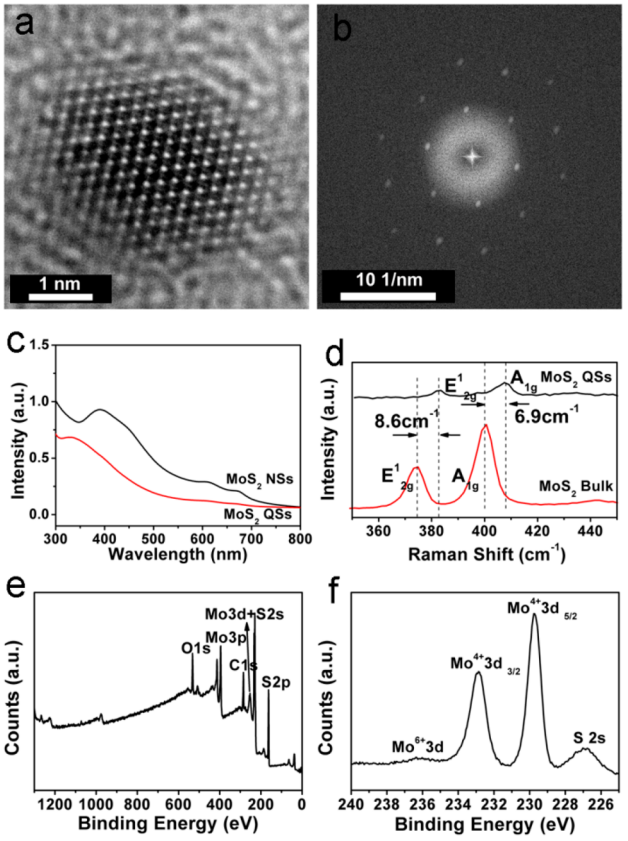

Figure 2. Structural elucidation of MoS_2 QSs. (a) HRTEM image and (b) the corresponding FFT pattern of a single MoS_2 QS. (c) UV−vis absorption spectra. (d) Raman spectra. (e) Full-scan and (f) partial-scan XPS spectra.

spectra, as shown in Figure 2d, both the bulk and QSs of MoS_2 showed peaks of A_{1g} and E^1_{2g} modes. Compared to those of the bulk, A_{1g} and E^1_{2g} peaks of the QSs were significantly weakened and blue-shifted. The A_{1g} peak was shifted from 400.6 to 407.5 cm^{-1}, and the E^1_{2g} peak was shifted from 374.9 to 383.5 cm^{-1}. Such a blue shift phenomenon was similar to the mode change of black phosphorus quantum dots with thickness and lateral size reduction.[10]

X-ray photoelectron spectroscopy (XPS) was performed to further identify the defect-free characteristics of the MoS_2 QSs. As shown in Figure 2e, peaks for Mo and S were observed, whereas no peaks for Na or Cl were found, indicating complete removal of the salts from the resulting QSs. Doublet peaks at 232.8 and 229.6 eV in Figure 2f corresponded to Mo^{4+} $3d_{3/2}$ and Mo^{4+} $3d_{5/2}$, respectively, of trigonal prismatic (2H) MoS_2. No octahedral (1T) MoS_2 was detected in the XPS spectrum. The trace amount of Mo^{6+} 3d at 235.6 eV might originate from the negligible oxidation of Mo edge atoms. Similarly, the XPS spectra (Figure S2) of the WS_2 QSs demonstrated the presence of 2H WS_2 and absence of 1T WS_2.[24]

From the above, the MoS_2 and WS_2 QSs produced from their bulk materials were intrinsic and defect-free. Meanwhile, high-yield production of such remarkable materials was achieved. Table S1 indicates that three prerequisites such as salt-assisted ball-milling, sufficient ball-milling time, and sonication-assisted solvent exfoliation had to be simultaneously fulfilled to achieve high production yield. For highlighting the salt-assisted ball-milling process, a series of SEM images were taken of the MoS_2 products after salts were removed (Figure S3). Clearly the lateral size and thickness of MoS_2 were steadily decreased with increasing ball-milling time. After sufficient time, e.g., 12 h, the pulverization proceeded to an unprecedented level (Figure S3e). Such significant pulverization could not be achieved when no salts were introduced during the ball-milling process (Figure S3b).[25] The progressive size reduction of the MoS_2 products was easier to observe in high-magnification SEM images (Figure S4). Similar trends were found in the case of WS_2 (Figure S5). A wide range of inorganic salts were testified to promote the pulverization of MoS_2 and WS_2 (Table S2). However, some salts, e.g., zinc acetate ($Zn(Ac)_2$), were not as promotive as the others. For determining the underlying cause, NaCl and $Zn(Ac)_2$ were separately subjected to ball-milling for 12 h. SEM images (Figure S6) were collected and compared, showing the distinct appearances between the two types of salt. NaCl remained crystalline with sharp edges, whereas $Zn(Ac)_2$ was deformed and severely agglomerated. Evidently, the durable crystallinity of the salts was determinative to achieve significant size reduction during the salt-assisted ball-milling process.

On the basis of the above results and analysis, a possible mechanism for the production of the QSs was proposed. Figure 3 presents a schematic illustration of such a mechanism. The

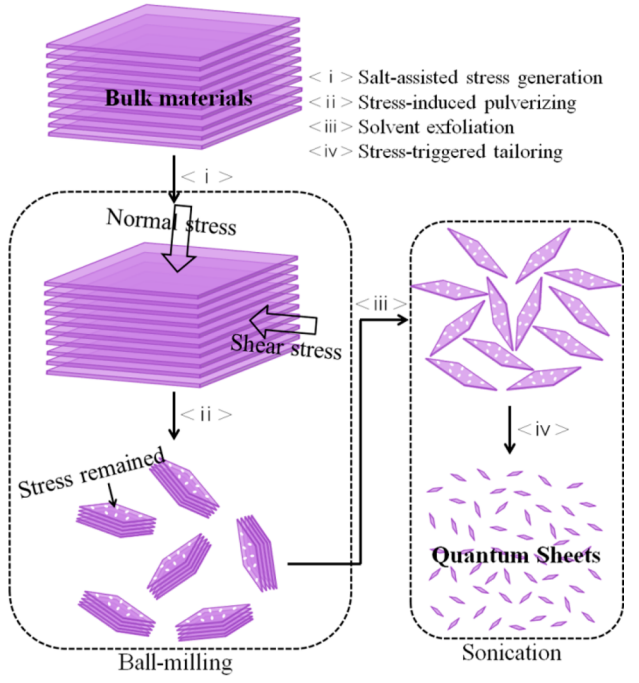

Figure 3. Schematic illustration of the proposed fabrication mechanism of MoS_2 and WS_2 QSs. Two methods (i.e., ball-milling and sonication) and four steps (i.e., salt-assisted stress generation, stress-induced pulverizing, solvent exfoliation, and stress-triggered tailoring) are involved in the fabrication process.

whole fabrication process underwent two stages, i.e., ball-milling and sonication. Starting from the bulk materials, the salt-assisted ball-milling introduced compression and shear forces simultaneously, which induced normal and shear stress, respectively, inside the bulk materials. The pulverization subsequently took place and was greatly promoted by the numerous stress points. The ball-milling and pulverization enabled the successive refreshing of the interfaces at the stress points. Consequently, the fracture and exfoliation continued

DOI: 10.1021/acs.nanolett.7b03968
Nano Lett. 2017, 17, 7767−7772

until an unprecedented level of size reduction was reached. However, the breakage of the remaining tough stress points was beyond the capacity of the pulverization by the salt-assisted ball-milling. The salts were then washed away from the pulverized materials. The following sonication-assisted solvent exfoliation further exfoliated the pulverized materials into a mono/few layers. Triggered by the remaining stress, the mono/few layers under sonication were tailored into the QSs. The sonication was powerful enough to break the remaining stress points so that intrinsic and defect-free QSs were obtained.

As mentioned before, sufficient ball-milling time was indispensable to achieve high production yield. Figure S7 demonstrates the dynamic evolution of the MoS_2 and NaCl mixtures with increasing ball-milling time. Compared with Figure S6, it could be judged that in Figure S7 the crystallites with smooth surfaces were NaCl. During the salt-assisted ball-milling process, the pulverization of MoS_2 proceeded progressively whereas the NaCl remained crystalline with average sizes of approximately 1−3 μm. The penetration of NaCl into MoS_2 became dominant when the ball-milling time reached 12 h. Assuming that the cubic crystallites of NaCl was the transfer media through the opposite faces for the compression forces between the milling balls and the MoS_2 surfaces (with average lengths of approximately 5 μm) and considering the force generation from the ball-milling at a running speed of 500 rpm, the calculated pressure on the MoS_2 surfaces was 4−36 GPa. It was reported that the MoS_2 breaking strength was approximately 16−30 GPa.[26] The NaCl crystallites could transfer the forces through the sharp edges and even the corners, which enabled the MoS_2 surfaces to eventually receive an average pressure well above the reported breaking strength. Clearly, both experimental evidence and theoretical calculations strongly supported the proposed fabrication mechanism.

Solution processing had been widely used for the fabrication of hybrid materials. To conduct solution-processing, the diversity and solvability of the solvents were the key factors. In this work, the remarkable diversity and extraordinary solvability of the solvents available for dispersion of the MoS_2 and WS_2 QSs are demonstrated in Figure 4. Starting from the original dispersion of the QSs in NMP, the redispersion process was schematically illustrated in Figure 4a. The QSs were precipitated in ethyl acetate and collected as dry powder. The following redispersion of the dry powder into a variety of solvents resulted in a wide range of redispersion systems. Figure 4b presented the photographs of the representative redispersion systems, e.g., MoS_2 QSs in NMP, dimethylformamide (DMF), acetone, ethanol, and water, which were highly stable with high concentrations of 20 mg/mL. Such solvent diversity and solvability would greatly facilitate the solution processing of the MoS_2 and WS_2 QSs. Figure 4c showed the stability of the initial dispersion and redispersion of MoS_2 QSs in NMP. Both initial dispersion and redispersion presented outstanding stability. For example, there was no observable change in the concentration of the dispersion system when standing still for 1 week. Redispersion of MoS_2 QSs in other solvents at 20 mg/mL also showed high stability, e.g., with constant concentration for at least 24 h. Figure 4d demonstrates the reversibility of the (re)dispersion-precipitation process of the MoS_2 QSs in NMP. Once observable precipitation occurred (e.g., standing still for >7 days or centrifugation at >6000 rpm), the (re)dispersion could be rapidly and completely recovered to its stable state by simple hand-shaking or vortex-mixing. Such stability and

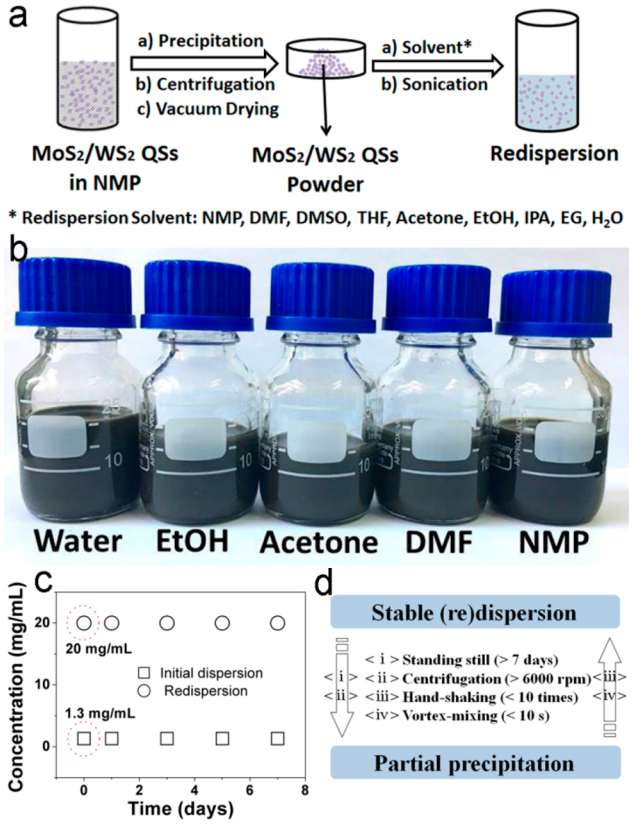

Figure 4. Redispersion of MoS_2 and WS_2 QSs in a wide range of solvents. (a) Schematic illustration of the redispersion process. (b) Photographs of the representative (MoS_2 QSs) redispersion systems with high concentrations (i.e., 20 mg/mL). (c) Stability of the initial dispersion and redispersion in NMP. (d) Reversibility of the (re)dispersion-precipitation process in NMP.

reversibility could bring great convenience to the practical applications of the QS dispersion.

As a demonstration, hybrid thin films were fabricated through solution-processing of the MoS_2 QSs/NSs and PMMA in NMP. The loading contents of the QSs could be exactly and widely modulated in the QSs-PMMA thin films (Figure S8). Depending on the solvent selected for the solution processing, a wide spectrum of polymers would be applicable as the matrix for the hybrid thin films. Figure 5a presents photographs of PMMA, QSs-PMMA, and NSs-PMMA thin films. Both QSs-PMMA and NSs-PMMA thin films were less transparent than PMMA. Despite the same loading content of 0.1 wt %, the QSs-PMMA thin film appeared more transparent than NSs-PMMA. The corresponding small-angle X-ray scattering (SAXS) images indicated that the QSs/NSs were uniformly and randomly dispersed in the PMMA matrix, and there were no detectable aggregation and orientation of the QSs/NSs in the hybrid thin films. Such distribution was further confirmed by the TEM image of the cross-section of the QSs-PMMA hybrid thin film, as shown in Figure 5b. Both SAXS and TEM suggested the high quality of the solution-processed hybrid thin films.

For demonstrating the optical properties of the hybrid thin films, linear and nonlinear absorption were measured. Figure 5c showed the UV−vis spectra of the PMMA, QSs-PMMA, and NSs-PMMA thin films. Apparently, the QSs-PMMA thin film was less absorptive than NSs-PMMA in the visible range, which led to better transparency for the former than the latter.

DOI: 10.1021/acs.nanolett.7b03968
Nano Lett. 2017, 17, 7767−7772

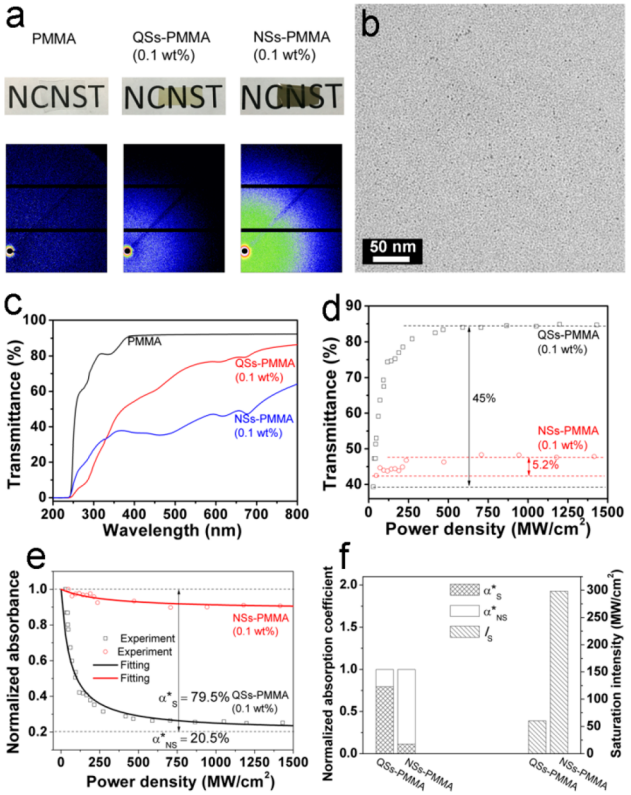

Figure 5. Optical properties of the (MoS_2) QSs-PMMA hybrid thin film. (a) (top panel) Photographs of the thin films; (bottom panel) corresponding SAXS images. (b) TEM image of the (QSs-PMMA) cross-section. (c) UV−vis absorption spectra. (d) Nonlinear saturable absorption curves. (e) Normalized absorption curves. The hollow dots are the experimental data, and the solid curves are analytical fits to the data. (f) Plots of the normalized absorption coefficient and saturation intensity. The incident laser beam was as follows: wavelength of 800 nm, pulse of 60 fs, and repetition rate of 1 kHz.

Considering that the thickness of the thin film was 10 μm, and assuming that the density of the thin film (0.1 wt %) was similar to that of pure PMMA (1.18×10^3 mg/mL), the linear absorption coefficient (at 800 nm) was calculated to be 1.2×10^4 and 3.1×10^4 mL mg^{-1} m^{-1} for the QSs-PMMA and NSs-PMMA, respectively, larger than those reported for MoS_2 dispersions.[27,28] Figure 5d presents the nonlinear saturable absorption curves of the QSs-PMMA and NSs-PMMA hybrid thin films with the femtosecond laser at an illumination wavelength of 800 nm. The QSs-PMMA thin film with loading content of merely 0.1 wt % demonstrated exceptional nonlinear absorption saturation with (absolute) modulation depth of approximately 45%, nearly an order of magnitude enhancement to that of NSs-PMMA. Such great enhancement in modulation depth was caused by the boost of nonlinear absorption saturation in the QSs compared with the NSs, which could be related to the sharp rise of quantum confinement and edge effects in the former compared with the latter, particularly at the same content. In addition, this was the first demonstration of such large modulation depth in 2D TMDs,[29−32] which would prompt the full exploration of the potential applications of the 2D QSs in photonics, lasers, and nonlinear optics. Figure 5e presents the normalized absorption curves of the QSs-PMMA and NSs-PMMA, respectively. The experimental data were perfectly fitted by using the following formula: $\alpha^*(I) = \alpha^*_S/(1 + I/I_S) + \alpha^*_{NS}$ where $\alpha^*(I)$ is the absorption coefficient, α^*_S and α^*_{NS} are the saturable and nonsaturable absorption components, I is the peak intensity (or power density) of the incident pulsed laser, and I_S is the saturation intensity defined as the optical intensity required in a steady state to reduce the absorption to half of its unbleached value.[31] From the fitting, the (relative) modulation depth (i.e., α^*_S) of nearly 80% could be derived for the QSs-PMMA. Figure 5f shows plots of the normalized absorption coefficient and saturation intensity. The QSs-PMMA demonstrated much larger saturable absorption coefficient (α^*_S) and significantly lower saturation intensity (I_S) than those of the NSs-PMMA, indicating the superior nonlinear absorption saturation of the former to the latter.

In summary, high-yield production of intrinsic and defect-free MoS_2 and WS_2 QSs were achieved through a sequential combination of salt-assisted ball-milling and sonication-assisted solvent exfoliation of the bulk materials. The production yield reproducibly exceeded 20 wt %, indicating the great competitiveness of our fabrication method toward mass production of the 2D QSs. The resulting QSs could be transferred from NMP to a wide range of solvents, and the redispersion concentration could reach up to 20 mg/mL or even higher. Such solvent diversity and solvability dramatically facilitated the solution-processing of the QSs. The demonstration of nearly an order of magnitude enhancement in modulation depth of nonlinear absorption saturation of the QSs-PMMA compared with the NSs-PMMA would greatly expedite the full exploration of the 2D QSs.

■ ASSOCIATED CONTENT

Supporting Information

The Supporting Information is available free of charge on the ACS Publications website at DOI: 10.1021/acs.nanolett.7b03968.

Experimental details and additional data (PDF)

■ AUTHOR INFORMATION

Corresponding Author

*E-mail: zhangyong@nanoctr.cn.

ORCID

Yong Zhang: 0000-0002-5914-1065

Xinfeng Liu: 0000-0002-7662-7171

Author Contributions

C.H. performed the experiments and characterizations. Y.Z. supervised the research project. C.H. and Y.Z. analyzed the data and wrote the manuscript. P.G. and S.C. performed HRTEM characterization. X.L. and Y.M. performed nonlinear optical characterization. J.Z. performed SAXS characterization. Y.M., W.J., and J.C. carried out the fabrication of hybrid thin films. All of the authors discussed the results and commented on the manuscript.

Notes

The authors declare no competing financial interest.

■ ACKNOWLEDGMENTS

This work was supported by the start-up funding from National Center for Nanoscience and Technology, the 100-Talent Program of Chinese Academy of Sciences, and a grant from the National Natural Science Foundation of China (No. 61575049).

DOI: 10.1021/acs.nanolett.7b03968
Nano Lett. 2017, 17, 7767−7772

REFERENCES

(1) Geim, A. K. *Science* **2009**, *324*, 1530−1534.
(2) Coleman, J. N.; Lotya, M.; O'Neill, A.; Bergin, S. D.; King, P. J.; Khan, U.; Young, K.; Gaucher, A.; De, S.; Smith, R. J.; Shvets, I. V.; Arora, S. K.; Stanton, G.; Kim, H. Y.; Lee, K.; Kim, G. T.; Duesberg, G. S.; Hallam, T.; Boland, J. J.; Wang, J. J.; Donegan, J. F.; Grunlan, J. C.; Moriarty, G.; Shmeliov, A.; Nicholls, R. J.; Perkins, J. M.; Grieveson, E. M.; Theuwissen, K.; McComb, D. W.; Nellist, P. D.; Nicolosi, V. *Science* **2011**, *331*, 568−571.
(3) Zhang, Y.; Magan, J. J.; Blau, W. J. *Sci. Rep.* **2014**, *4*, 4822.
(4) Rao, C. N. R.; Matte, H. S. S. R.; Maitra, U. *Angew. Chem., Int. Ed.* **2013**, *52*, 13162−13185.
(5) Baringhaus, J.; Ruan, M.; Edler, F.; Tejeda, A.; Sicot, M.; Taleb-Ibrahimi, A.; Li, A. P.; Jiang, Z.; Conrad, E. H.; Berger, C.; Tegenkamp, C.; de Heer, W. A. *Nature* **2014**, *506*, 349−354.
(6) Wang, X.; Sun, G.; Li, N.; Chen, P. *Chem. Soc. Rev.* **2016**, *45*, 2239−2262.
(7) Moon, J.; An, J.; Sim, U.; Cho, S. P.; Kang, J. H.; Chung, C.; Seo, J. H.; Lee, J.; Nam, K. T.; Hong, B. H. *Adv. Mater.* **2014**, *26*, 3501−3505.
(8) Shen, J.; Zhu, Y.; Yang, X.; Li, C. *Chem. Commun.* **2012**, *48*, 3686−3699.
(9) Xu, S.; Li, D.; Wu, P. *Adv. Funct. Mater.* **2015**, *25*, 1127−1136.
(10) Zhang, X.; Xie, H.; Liu, Z.; Tan, C.; Luo, Z.; Li, H.; Lin, J.; Sun, L.; Chen, W.; Xu, Z.; Xie, L.; Huang, W.; Zhang, H. *Angew. Chem., Int. Ed.* **2015**, *54*, 3653−3657.
(11) Wang, Q. H.; Kalantar-Zadeh, K.; Kis, A.; Coleman, J. N.; Strano, M. S. *Nat. Nanotechnol.* **2012**, *7*, 699−712.
(12) Laursen, A. B.; Kegnaes, S.; Dahl, S.; Chorkendorff, I. *Energy Environ. Sci.* **2012**, *5*, 5577−5591.
(13) Cheng, L.; Liu, J.; Gu, X.; Gong, H.; Shi, X.; Liu, T.; Wang, C.; Wang, X.; Liu, G.; Xing, H.; Bu, W.; Sun, B.; Liu, Z. *Adv. Mater.* **2014**, *26*, 1886−1893.
(14) Chhowalla, M.; Shin, H. S.; Eda, G.; Li, L. J.; Loh, K. P.; Zhang, H. *Nat. Chem.* **2013**, *5*, 263−275.
(15) Gu, W.; Yan, Y.; Zhang, C.; Ding, C.; Xian, Y. *ACS Appl. Mater. Interfaces* **2016**, *8*, 11272−11279.
(16) Zhang, X.; Lai, Z.; Liu, Z.; Tan, C.; Huang, Y.; Li, B.; Zhao, M.; Xie, L.; Huang, W.; Zhang, H. *Angew. Chem., Int. Ed.* **2015**, *54*, 5425−5428.
(17) Huang, X.; Zeng, Z.; Zhang, H. *Chem. Soc. Rev.* **2013**, *42*, 1934−1946.
(18) Yao, Y.; Tolentino, L.; Yang, Z.; Song, X.; Zhang, W.; Chen, Y.; Wong, C. P. *Adv. Funct. Mater.* **2013**, *23*, 3577−3583.
(19) Lee, D.; Lee, B.; Park, K. H.; Ryu, H. J.; Jeon, S.; Hong, S. H. *Nano Lett.* **2015**, *15*, 1238−1244.
(20) Lei, W.; Mochalin, V. N.; Liu, D.; Qin, S.; Gogotsi, Y.; Chen, Y. *Nat. Commun.* **2015**, *6*, 8849.
(21) Jeon, I. Y.; Shin, Y. R.; Sohn, G. J.; Choi, H. J.; Bae, S. Y.; Mahmood, J.; Jung, S. M.; Seo, J. M.; Kim, M. J.; Chang, D. W.; Dai, L.; Baek, J. B. *Proc. Natl. Acad. Sci. U. S. A.* **2012**, *109*, 5588−5593.
(22) Posudievsky, O. Y.; Khazieieva, O. A.; Cherepanov, V. V.; Dovbeshko, G. I.; Shkavro, A. G.; Koshechko, V. G.; Pokhodenko, V. D. *J. Mater. Chem. C* **2013**, *1*, 6411−6415.
(23) Gan, Z. X.; Liu, L. Z.; Wu, H. Y.; Hao, Y. L.; Shan, Y.; Wu, X. L.; Chu, P. K. *Appl. Phys. Lett.* **2015**, *106*, 233113.
(24) Voiry, D.; Yamaguchi, H.; Li, J.; Silva, R.; Alves, D. C. B.; Fujita, T.; Chen, M.; Asefa, T.; Shenoy, V. B.; Eda, G.; Chhowalla, M. *Nat. Mater.* **2013**, *12*, 850−855.
(25) Ambrosi, A.; Chia, X.; Sofer, Z.; Pumera, M. *Electrochem. Commun.* **2015**, *54*, 36−40.
(26) Bertolazzi, S.; Brivio, J.; Kis, A. *ACS Nano* **2011**, *5*, 9703−9709.
(27) O'Neill, A.; Khan, U.; Coleman, J. N. *Chem. Mater.* **2012**, *24*, 2414−2421.
(28) Paton, K. R.; Coleman, J. N. *Carbon* **2016**, *107*, 733−738.
(29) Du, J.; Wang, Q.; Jiang, G.; Xu, C.; Zhao, C.; Xiang, Y.; Chen, Y.; Wen, S.; Zhang, H. *Sci. Rep.* **2014**, *4*, 6346.
(30) Mao, D.; Wang, Y.; Ma, C.; Han, L.; Jiang, B.; Gan, X.; Hua, S.; Zhang, W.; Mei, T.; Zhao, J. *Sci. Rep.* **2015**, *5*, 7965.
(31) Bao, Q.; Zhang, H.; Wang, Y.; Ni, Z.; Yan, Y.; Shen, Z. X.; Loh, K. P.; Tang, D. Y. *Adv. Funct. Mater.* **2009**, *19*, 3077−3083.
(32) Zhang, Y.; Wang, J. J.; Ballantine, K. E.; Eastham, P. R.; Blau, W. J. *Adv. Opt. Mater.* **2014**, *2*, 331−337.

DOI: 10.1021/acs.nanolett.7b03968
Nano Lett. 2017, 17, 7767−7772